Check for updates

Pd nanocatalysts adsorbed onto silica nanoparticle coated indium tin oxide: a reusable nanozyme for glucose detection†

Ridge Chavalala [ID] [a] and Philani Mashazi [ID] ⋆[ab]

Nanozymes are nanomaterials that exhibit enzyme-like activity upon exposure to a substrate solution. The use of noble and platinum group metals enhances enzyme-like catalytic activity. However, noble metals are obtained at a high cost; therefore, their recovery after use is of high importance. Herein, we report the fabrication of indium tin oxide–silica nanoparticles decorated with palladium nanoparticles (ITO-SiO$_2$-prS-PdNPs). The ITO-SiO$_2$-prS-PdNPs were evaluated for peroxidase-like activity toward the oxidation of 3,3′,5,5′-tetramethylbenzidine (TMB) in the presence of H$_2$O$_2$. A colour change from clear or colourless TMB to blue colour (oxidized TMB products) was observed confirming the peroxidase-like activity. A typical Michaelis–Menten enzyme-like behaviour is observed with K_m values of 0.68 mM for H$_2$O$_2$ and 0.47 mM for TMB, which are better than the reported values for horse-radish peroxidase (HRP) for the same substrate. The peroxidase-like activity of ITO-SiO$_2$-prS-PdNPs was found to proceed *via* the electron-transfer mechanism. The ITO-SiO$_2$-prS-PdNPs were cleaned successfully after each use by rinsing with water and ethanol solution thus making the surface simple and easy to recover and reuse. A reusable and highly selective colorimetric assay for glucose detection based on the peroxidase-like activity of ITO-SiO$_2$-prS-PdNPs gave excellent results. ITO-SiO$_2$-prS-PdNPs exhibited a good linear range of 5.0–30 μM, a low limit of detection (LOD) of 1.84 μM and a limit of quantification (LOQ) of 6.14 μM. Finally, the nanozyme (ITO-SiO$_2$-prS-PdNPs) was successfully used to detect glucose in a complex newborn calf serum (NCS), representing a real sample.

1. Introduction

Glucose plays an important role in living cells as a metabolic intermediate and as a source of energy.[1,2] It has been reported that normal levels of glucose enhance communication between cells, increase memory and stimulate calcium absorption.[3] However, excessive glucose level is one of the main causes of diabetes.[4] The international diabetes federation (IDF) estimated that over 420 million people currently suffer from diabetes.[5,6] The global threats imposed by diabetes and its complications were a motivation behind this study.

The conventional detection and monitoring of glucose is based on personal glucose meters (PGMs). Recently, colorimetric sensors using chromogenic agents have been used.[7] PGMs utilize a glucose oxidase (GOx) enzyme to detect glucose. Glucose is oxidized by the GOx enzyme to produce D-gluconolactone which undergoes

spontaneous hydrolysis to form gluconic acid. During glucose oxidation, the GOx enzyme cofactor (FAD) is reduced to GOx-FADH$_2$ which is an unnatural state. The enzyme GOx (FADH$_2$) in the presence of oxygen is oxidized to GOx (FAD). Simultaneously, hydrogen peroxide (H$_2$O$_2$) is produced as an enzymatic reaction by-product. Colorimetric sensors have received research attention due to their simplistic operation and the results are visible to the naked eye as blue coloured products. In colorimetric sensing, H$_2$O$_2$ is reduced to reactive oxygen radical species (ROS) by nanomaterials.[8] ROS oxidizes a chromogen (TMB) to blue-coloured products. Other chromogenic species can also be used as long as they produce coloured products that are observable using naked eyes and can also be monitored using UV-vis spectroscopy.[9] A horse-radish peroxidase (HRP) enzyme can be used to monitor the colorimetric oxidation of TMB to coloured products. However, this will be an expensive bi-enzyme system. Natural enzymes have numerous limitations such as low stability under extreme conditions. The loss of stability for natural enzymes is expected at high pH, temperature, and humidity. Natural enzymes are costly to obtain in high purity. Natural enzymes denature under storage, and thus hindering their widespread applications.[10]

a Department of Chemistry, Rhodes University, PO Box 94, Makhanda, 6140, South Africa. E-mail: p.mashazi@ru.ac.za; Tel: +27 46 603 8846

b Institute for Nanotechnology Innovation, Rhodes University, PO Box 94, Makhanda, 6140, South Africa

This journal is © The Royal Society of Chemistry 2023

J. Mater. Chem. B, 2023, **11**, 7961–7971 | **7961**

Nanomaterials are emerging as the most promising substitutes for natural enzymes for biosensor fabrication and applications. They have been shown to exhibit enzyme-like activity and excellent environmental stability.[11] The enzyme-like activity of nanomaterials has been shown to mimic peroxidase, catalase and also superoxide dismutase-like activity.[12] The differences in the enzyme that nanomaterials mimic are influenced by the mechanism of action and the products they produce. Some nanomaterials have the ability to catalytically reduce hydrogen peroxide to reactive oxygen radical species (ROS). A series of noble metal nanoparticles (NPs), such as gold,[13] palladium,[14] platinum,[15] and silver,[16] have been investigated for their direct electrocatalytic oxidation of glucose. Enhanced catalytic activity was observed when small gold nanoparticles were introduced in the aerobic oxidation of glucose.[17] Combining two monometallic nanoparticles of AuNPs and AgNPs produced bimetallic (AuNPs–AgNPs) nanoparticles with improved catalytic activity and excellent optical properties for the colorimetric detection of glucose.[17] The ratiometric detection based on nanozymes such as MIL-88, magnetic nanoporous graphene (MNPG), and Mn_3O_4NPs has been used for the detection and monitoring of ascorbic acid (AA), glutathione, and dopamine, respectively.[18–20] The use of nanoparticles in solution show excellent results; however, their recovery and reuse still remain a world-wide research challenge.

We recently reported the use of magnetic nanoparticles with silica shells decorated with Au@PdNPs as the method to recover the nanocatalysts magnetically.[21] This study showed excellent results and the nanoparticles could be reused. The adsorption of metal nanoparticles on a solid support would also be beneficial for the recovery of nanocatalysts for further use. An easier method for nanocatalyst recovery is the attachment onto the solid support. Indium tin oxide (ITO) functionalized with silica nanoparticles has been reported to yield excellent nanocatalyst attachment.[22] ITO is a good conductor. Upon coating with silica nanoparticles, ITO becomes inert and thus an excellent catalyst support. Herein, we report the fabrication of indium tin oxide substrates first to form hydroxylated ITO (ITO-OH) for the attachment of inert silica nanoparticles (SiO_2NPs), thus forming $ITO-SiO_2NPs$. Palladium nanoparticles (PdNPs) were dispersed *via* 3-mercaptoproyl triethoxysilane (MPTES) to form $ITO-SiO_2$-prS-PdNPs. The $ITO-SiO_2$-prS-PdNP surface was evaluated for its properties as a potential nanozyme (peroxidase mimic) towards the oxidation of TMB in the presence of H_2O_2. A feasible approach with high selectivity and specificity towards the colorimetric detection of glucose was also investigated.

2. Experimental

2.1 Materials and reagents

Palladium chloride ($PdCl_2$), tetraethylorthosilicate (TEOS), sodium borohydride ($NaBH_4$), glacial acetic acid (CH_3COOH), 3,3′,5,5′-tetramethylbenzidine (TMB), 3-mercaptoproyl triethoxysilane (MPTES), D-glucose (Glu) powder, glucose oxidase (GOx, EC 1.1.3.4 from Aspergillus, Type VII), fructose (Fru), sucrose (Suc), lactose (Lac), 1,3-phenylisobenzofuran (DPBF), terephthalic acid (TA) and indium tin oxide (ITO) substrates were purchased from Sigma Aldrich. Hydrochloric acid (32% HCI), ammonium hydroxide (NH_4OH), ethanol (EtOH), and methanol (MeOH) were purchased from B&M Scientific. Disodium hydrogen orthophosphate (Na_2HPO_4) and sodium dihydrogen orthophosphate (NaH_2PO_4) were purchased from Associated Chemical Enterprises (ACE Chemicals). All the reagents were of analytical grade. All aqueous solutions were prepared using ultrapure water with a resistivity of 18.2 ΩM.cm obtained using a MilliQ system (Millipore, Corp, Bedford, MA, USA).

2.2 Apparatus

UV-vis measurements were carried out using a Thermo-Scientific, Multiskan Sky w Cuvette and touch screen, 100–240 V, Belgium. Fourier transform infrared spectroscopy (FTIR) measurements were carried out using a Perkin Elmer spectrum 100 FTIR spectrometer. The hydrodynamic and zeta potential measurements were carried out using a Malvern Zetasizer Nano-ZS90 series equipped with a 633 nm He/Ne laser. A disposable folded capillary cell (DTS 1060) was used for data collection for zeta potential measurements. Transmission electron microscopy (TEM) micrographs were obtained using a Zeiss Libra 120 TEM operating at 80 kV. The nanoparticles were dissolved in water and dropped onto a carbon-coated copper grid, and allowed to dry overnight at room temperature before measurements. Scanning electron microscopy (SEM) and energy dispersive X-ray spectroscopy (SEM-EDX) images and elemental compositions were obtained using an INCA PENTA FET coupled with VEGA TESCAN at 20 kV acceleration voltage. X-ray diffraction (XRD) patterns were recorded using a Bruker D8 Discover diffractometer equipped with a Lynx Eye detector, using Cu-Kα radiation (1.5405 Å, nickel filter). The samples were placed on a silicon wafer slide. The data were collected in the range from $2\theta = 10°$ to $100°$. X-ray photoelectron spectroscopy (XPS) measurements were conducted using an XPS from Kratos - DLD Ultra, UK. The vision processing 2 software was used for the elemental composition and fitting of the high-resolution spectra. Electrochemical measurements were performed using an Autolab Galvanostat/Potentiostat 302N workstation controlled by a Proline computer running on NOVA 1.10 software.

2.3 Preparation of silica nanoparticles (SiO_2NPs)

The preparation of silica NPs (SiO_2NPs) was achieved using a Stöber method.[23] Briefly, 15 mL NH_4OH was added into 250 mL EtOH and the mixture was heated at 40 °C with stirring at 200 rpm for 30 min. TEOS (2.5 mL) was added and the mixture was left to react for 12 hours with constant stirring at 40 °C. Additionally, 1.25 mL of TEOS was added at an interval of one hour for 12 hours to grow a silica shell. A translucent milky solution was obtained indicating the formation of silica nanoparticles (SiO_2NPs). The solution was centrifuged and washed several times with ethanol and deionized water.

7962 | *J. Mater. Chem. B*, 2023, **11**, 7961–7971

This journal is © The Royal Society of Chemistry 2023

2.4 Preparation of palladium nanoparticles (PdNPs)

The preparation of palladium NPs (PdNPs) was achieved using sodium borohydride ($NaBH_4$) reduction of H_2PdCl_4 and following a reported method, with slight changes.[24] Briefly, the palladium (II) hydrogen chloride precursor (H_2PdCl_4) was obtained by dissolving $PdCl_2$ (1 mM) with hydrochloric acid (32%, 10 mL) in 100 mL of deionized water under stirring for 3 hours. The obtained H_2PdCl_4 solution was yellowish in colour. An ice-cold 0.50 mL of $NaBH_4$ (0.026 M, 1.0 mg) was added into the H_2PdCl_4 solution dropwise over 30 min under stirring. As $NaBH_4$ was added, the yellow solution of H_2PdCl_4 turned black. The colour change signified the formation of palladium nanoparticles (PdNPs). The solution was centrifuged and washed several times with deionized water and the obtained precipitate was air-dried at room temperature.

2.5 Fabrication of ITO-SiO$_2$-prS-PdNPs, Scheme 1

The preparation of ITO-SiO$_2$-prS-PdNPs was achieved following the method described in Scheme 1. An appropriately cleaned bare ITO substrate (transparent conducting oxides) was hydroxylated in the mixture of $NH_4OH:H_2O_2:H_2O$ in the ratio of $1:1:5$ at 60 °C for 30 min in an oven to form the hydroxyl ITO surface (ITO-OH). SiO$_2$NPs (2.0 mg mL^{-1}) in ethanol were coated onto ITO-OH for 24 hours to form ITO-SiO$_2$NPs. Covalent bonds between the ITO-OH substrate and silanol (Si–OH) of SiO$_2$NP groups resulted in the formation of siloxane (Si–O–Si) functional groups and loss of H_2O. Attachment of SiO$_2$NPs resulted in an increase in the surface area of the flat ITO to form ITO-SiO$_2$NPs. MPTES (40 mM) in ethanol was used to modify the ITO-SiO$_2$NPs and to form thiol-functionalized ITO-SiO$_2$-prSH and this reaction took 3 hours. The terminal –SH bonds on ITO-SiO$_2$-prSH served as an anchor for the chemisorption of the noble metal NPs. Aqueous solution PdNPs (2.0 mg mL^{-1}) were dispersed using ultrasonication. ITO-SiO$_2$-prSH was immersed in the dispersed PdNP solution to form ITO-SiO$_2$-prS-PdNPs in 24 hours. The ITO-SiO$_2$-prS-PdNPs were rinsed with water to remove physically adsorbed PdNPs and dried with N_2 gas. The colour of the ITO-SiO$_2$-prS-PdNPs was blackish, confirming the successful deposition of PdNPs.

2.6 Peroxidase-like activity of ITO-SiO$_2$-prS-PdNPs

The catalytic oxidation of TMB in the presence of H_2O_2 was investigated at room temperature (25 °C). Briefly, ITO-SiO$_2$-prS-PdNPs (0.50 cm × 1.0 cm), H_2O_2 (0.20 M, 200 μL), TMB (4.2 mM, 200 μL) and acetate buffer (pH 4.0, 0.20 M) were incubated together for 15 min. A blue colour was observed and monitored using a UV-vis spectrophotometer and the measured wavelength was between 300 and 800 nm.

2.7 Colorimetric detection of glucose

Glucose detection was performed by following these steps: (a) 100 μL of GOx (4 mg mL^{-1}) and 200 μL of glucose with different concentrations in 0.010 M PBS (pH 7.0) were incubated at 37 °C. The reaction was allowed to take place for 45 min. (b) To this solution, 100 μL of 2.0 mM TMB and ITO-SiO$_2$-prS-PdNPs in 0.20 M acetate buffer (pH 4.0) were added and incubated at 37 °C for 15 min. An increase in the absorption band at 652 nm was observed and monitored using a UV-vis spectrophotometer. Each concentration of glucose was measured in triplicates ($n = 3$) and average absorption spectra were recorded. The percentage relative standard deviation (%RDS) was also calculated from the measurements.

2.8 Evaluating ROS generation using a radical scavenger

The two studies were conducted:

(i) 1,3-Diphenylisobenzofuran (DPBF) has an absorption at 420 nm. Upon reacting with reactive oxygen radical species (ROS), the absorption decreases and this can be monitored using a UV-vis spectrophotometer. Experimentally, ITO-SiO$_2$-prS-PdNPs were immersed in 1 mL of acetate buffer (pH 4.0) solution of H_2O_2 (5.0 mM) followed by the addition of 200 μL of 0.25 mM DPBF (also in acetate buffer pH 4.0). The UV-vis spectra were recorded for 10 minutes at 1 minute interval. The initial solution of 200 μL of 0.25 mM DPBF was diluted in 1 mL of acetate buffer and measured fresh after preparation. Also, we allowed the reaction to stand for 10 min and measured.

(ii) Terephthalic acid, TA (a fluorescence hydroxyl radical quencher) was used in the presence of ITO-SiO$_2$-prS-PdNPs

Scheme 1   Step-by-step fabrication of ITO–SiO$_2$–prS–PdNPs as described in Section 2.5.

This journal is © The Royal Society of Chemistry 2023

J. Mater. Chem. B, 2023, 11, 7961–7971 | 7963

Paper

and H_2O_2. The reaction mixture of 1.0 mM TA in ethanol (1 mL) with acetate buffer (pH 4.0, 4 mL) was mixed with ITO-SiO$_2$-prS-PdNPs in the presence of 3.0 mM H_2O_2 and incubated for 10 min. Fluorescence emission spectra excited at 320 nm were recorded.

2.9 Electrochemical measurements

All electrochemical experiments were studied using a three-electrode system with ITO-SiO$_2$-prS-PdNPs as the working electrode, the coiled platinum wire as the counter electrode and Ag|AgCI as the pseudo-reference electrode in acetate buffer pH 4.0 at room temperature. The electrocatalytic oxidation of

ITO-SiO$_2$-prS-PdNPs toward H_2O_2 was performed using the amperometric technique and +0.50 V applied potential.

3. Results and discussion

3.1 Characterization of SiO$_2$NPs

The TEM image of SiO$_2$NPs in Fig. S1(a) (ESI†) shows spherical monodispersed nanoparticles. The particle size distribution in Fig. S1(b) (ESI†) of SiO$_2$NPs was 72.0 ± 7.5 nm. The FT-IR spectrum in Fig. S1(c) (ESI†) shows the characteristic peaks of silica at 793, 952, and 1063 cm^{-1} assigned to siloxane (Si–O–Si) symmetric stretching, silanol (Si–OH) stretching, and Si–O–Si
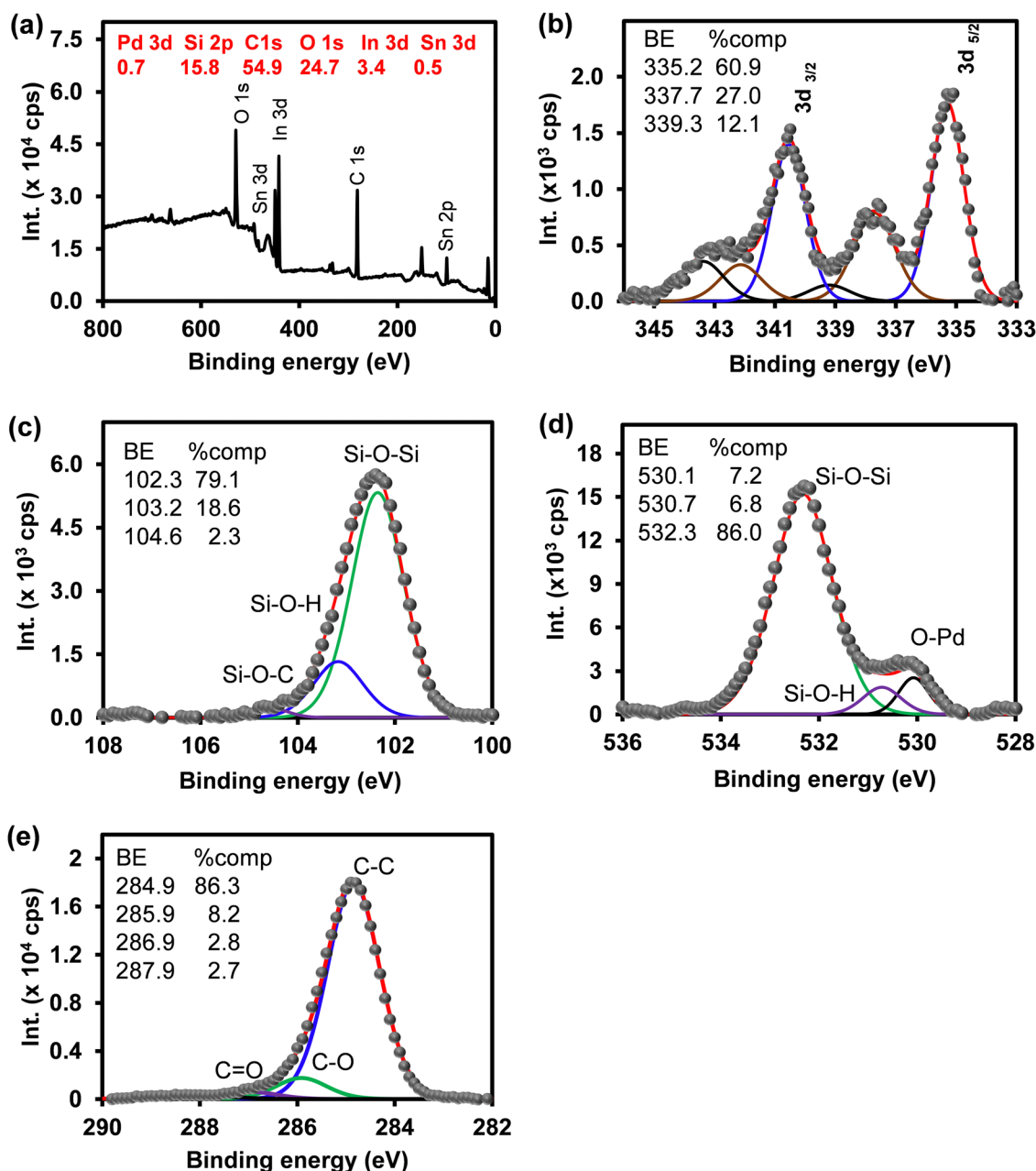

Fig. 1 (a) Survey spectrum and high-resolution spectra of (b) Pd 3d, (c) Si 2p, (d) O 1s, and (e) C 1s of ITO-SiO$_2$-prS-PdNPs.

asymmetric stretching vibrations, respectively. The peak at 3235 cm^{-1} is assigned to the O–H stretching of the silanol group. The EDX analysis in Fig. S1(d) (ESI†) shows the elemental composition of SiO$_2$NPs which showed the presence of Si K, O K, and C K with 40.3%, 57.2% and 2.5%, respectively. DLS was used to measure the particle size which was 78.0 nm in Fig. S1(e) (ESI†) and close to the TEM nanoparticle size.

3.2 Characterization of PdNPs

The TEM image in Fig. S2(a) (ESI†) exhibited agglomeration of the nanoparticles and this is due to the oxide species on the surface leading to particle–particle interaction. The particle size distribution in Fig. S2(b) (ESI†) showed that the palladium nanoparticles had a size of 7.9 ± 1.2 nm. The EDX spectrum in Fig. S2(c) (ESI†) shows the elemental composition of PdNPs and the presence of Pd M, O K and C K with 97.8%, 1.7% and 0.5%, respectively. The DLS diameter in Fig. S2(d) (ESI†) was 15.7 nm. The nanoparticle size diameter of DLS was higher than that in Fig. S2(b) (ESI†) and this was due to agglomeration as observed in the TEM image. The formation of PdNPs was also confirmed using XRD in Fig. S2(e) (ESI†). A diffraction pattern at the following 2θ (degree) values with their Miller indices in brackets 38.8° (111), 44.9° (200), 64.8° (202), 78.3° (311) and 81.4° (222), matching with a Pd JCPDS (05-0681). The Miller indices confirmed the presence of metallic Pd with a face-centered cubic (FCC) structure.

3.3 Characterization of the fabricated substrate, ITO-SiO$_2$-prS-PdNPs

The elemental composition of ITO-SiO$_2$-prS-PdNPs was investigated using EDX. Fig. S3 (ESI†) shows the EDX spectra of (a) bare ITO and (b) ITO-SiO$_2$-prS-PdNPs. The component compositions are displayed as the inset. The EDX spectrum of ITO showed the composition of a glass slide (substrate) with silicone (Si K), oxygen (O K) and metal ions (Mg K, Ca K, Al K, and Na K) that form a part of the glass. In addition, the glass substrate showed the presence of In M and Sn M due to the thin conducting layer. The EDX spectrum of ITO-SiO$_2$-prS-PdNPs confirmed the presence of Pd M (24.5%), due to the successful deposition of PdNPs onto ITO-SiO$_2$-prSH together with other elements from the ITO substrate.

In addition, XPS was used as a reliable quantitative technique to investigate the composition and oxidation states of Pd on the ITO-SiO$_2$-prS-PdNP surface. The survey spectrum in Fig. 1(a) confirmed the presence of Pd 3d (0.7%), Si 2p (15.8%), O 1s (24.7%), and C 1s (54.9%) as the elements of interest. Furthermore, ITO-SiO$_2$-prS-PdNPs showed the presence of In 3d (3.4%) and Sn 3d (0.5%) which were attributed to the underlying ITO surface. The difference in quantitative results between XPS and EDX is due to the fact that XPS has a low-depth resolution in nm compared to μm for EDX. Fig. 1(b) shows the high-resolution spectrum of Pd 3d with Pd^0 at 337.7 eV (21.6%) and Pd^{2+} oxidation states at 335.2 eV (32.9%), 340.5 eV (26.8) and at 342.9 eV (18.7%). The spin–orbit coupling of 5.26 eV was observed for Pd components at higher binding energies. Other high-resolution spectra of Si 2p

in Fig. 1(c), O 1s in Fig. 1(d) and C 1s in Fig. 1(e) are from the SiO$_2$NPs which was used as the adsorbent for PdNPs. The component assignments and composition are displayed as the inset in the figure.

3.4 Peroxidase-like activity of ITO-SiO$_2$-prS-PdNPs

The peroxidase-like activity of ITO-SiO$_2$-prS-PdNPs was investigated by the oxidation of TMB with H$_2$O$_2$. In Fig. 2, the reaction between (i) H$_2$O$_2$ + ITO-SiO$_2$-prS-PdNPs and (ii) TMB + ITO-SiO$_2$-prS-PdNPs showed clear solutions. The UV-vis spectrum of TMB + ITO-SiO$_2$-prS-PdNPs showed a small absorption peak at 652 nm and this is due to the oxidation of TMB as it is the light sensitive compound. Fig. 2(iii) shows ITO-SiO$_2$-prS-PdNPs in the presence of H$_2$O$_2$ and TMB. The solution turned blue in colour and this was accompanied by an increase in the absorption peaks at 370 nm and 652 nm. This confirms that ITO-SiO$_2$-prS-PdNPs possess the peroxidase-like activity. PdNPs exhibited higher peroxidase-like activity than ITO-SiO$_2$-prS-PdNPs as shown in Fig. S4 (ESI†). This was attributed to the rapid catalytic components of PdNPs in solution compared to the absorbed PdNPs onto the ITO-SiO$_2$-prSH surface. The bare ITO and ITO-SiO$_2$NPs did not show peroxidase-like activity. Therefore, the peroxidase-like activity was dependent on the presence of PdNPs adsorbed onto ITO-SiO$_2$-prSH as nanocatalysts. The results further confirmed that both TMB and H$_2$O$_2$ are necessary for the peroxidase-like activity of ITO-SiO$_2$-prS-PdNPs. This behaviour was similar to that observed for the commonly used horse-radish peroxidase (HRP) enzyme for the oxidation of TMB in the presence of H$_2$O$_2$.[25]

3.5 Effect of conditions on the peroxidase-like activity of ITO-SiO$_2$-prS-PdNPs

The peroxidase-like activity of ITO-SiO$_2$-prS-PdNPs was investigated under different environmental conditions, such as pH, reaction time, concentrations of H$_2$O$_2$ and TMB, and temperature. Fig. 3 shows the effect of (a) pH (2–6), (b) time (5–50 min)
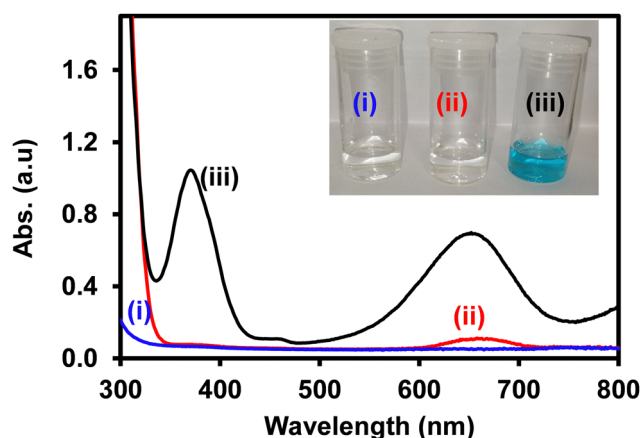

Fig. 2 UV-vis absorption spectra of (i) 0.20 M H$_2$O$_2$ + ITO-SiO$_2$-prS-PdNPs, (ii) 4.2 mM TMB + ITO-SiO$_2$-prS-PdNPs and (iii) 0.20 M H$_2$O$_2$ + 4.2 mM TMB + ITO-SiO$_2$-prS-PdNPs (The inset photograph for the corresponding colour change of different reaction systems). All were measured in 0.20 M acetate buffer (pH 4.0).
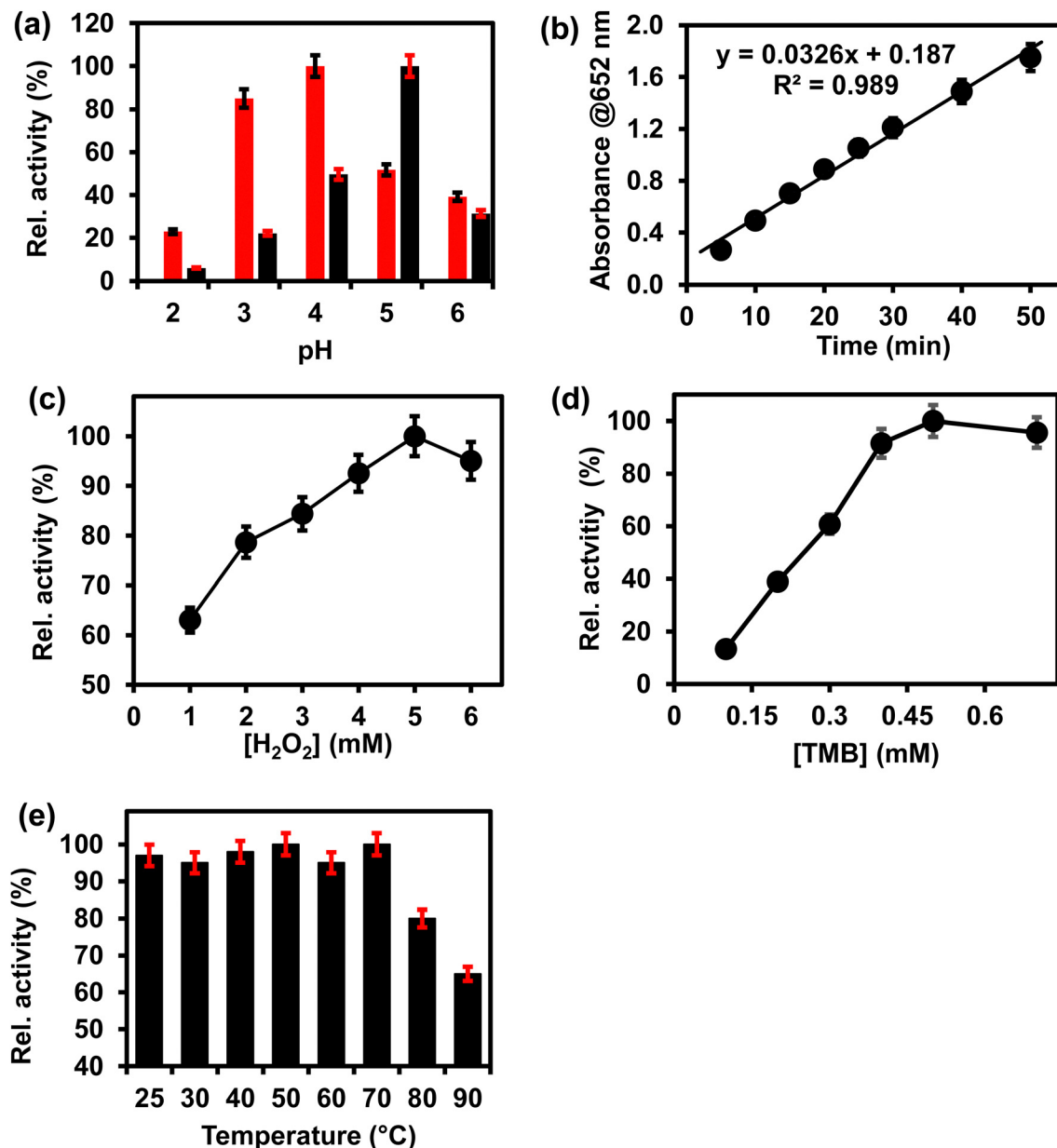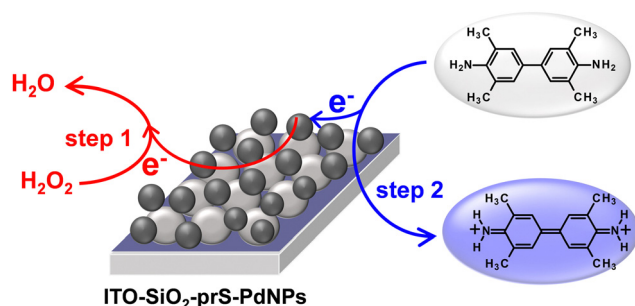
Fig. 3 Effect of (a) pH (red), (b) reaction time and changing concentrations of (c) H_2O_2 and (d) TMB, and (e) temperature on the peroxidase-like activity of ITO-SiO$_2$-prS-PdNPs. (Effect of pH (a) (black) on the peroxidase-like activity of PdNPs).

(c) [H_2O_2] (1–6 mM), (d) [TMB] (0.1–0.7 mM), and temperature (25–90 °C) on ITO-SiO$_2$-prS-PdNPs. Fig. 3(a) (red) shows that pH 4.0 gave the highest absorption intensity at 652 nm. This was due to the acidity of SiO$_2$NPs as a catalyst support thus allowing for PdNPs to be retained on the thiolated surface and the SiO$_2$NPs remained intact.[21] The absorption intensity at 652 nm increased from pH 2.0 to pH 4.0. The intensity decreased after pH 4.0. Under acidic conditions, H_2O_2 remains stable thus allowing for catalytic reduction. PdNPs on ITO-SiO$_2$-prS-PdNPs participate in the catalytic reduction of H_2O_2 to form radicals ($O_2^{-•}$, $HO_2^{-•}$ and $HO^{-•}$), which can oxidize TMB.[26] The optimum pH for the peroxidase-like activity of pure PdNPs not coated onto the ITO in Fig. 3(a) (black) was 5. Fig. 3(b)

shows that the blue colour intensity increased as the time continued and due to 3,3′,5,5′-tetramethylbenzidine diamine (TMBDI) products by ITO-SiO$_2$-prS-PdNPs and H_2O_2. Oxidized TMB formed a strong blue colour and the intensity of the reaction increased from 5 to 50 min. The regression equation for the reaction time was Abs_{652} = 0.0326x + 0.187 with a R^2 value of 0.989. The catalytic process of 15 min was selected for further investigations. An increase in absorption at 652 nm was observed as the concentration of H_2O_2 increased, Fig. 3(c), and also as the concentration of TMB increased, Fig. 3(d). At higher concentrations of H_2O_2 (>5.0 mM), a drastic decrease in absorption was observed. For TMB, a plateau was observed at [TMB] > 0.50 mM. The plateau and a decrease in intensity were

7966 | *J. Mater. Chem. B*, 2023, **11**, 7961–7971

This journal is © The Royal Society of Chemistry 2023

Scheme 2 ITO-SiO$_2$-prS-PdNP electron-transfer mechanism for TMB oxidation in 10 mM acetate buffer (pH 4.0).

attributed to the saturation of catalytic sites on the ITO-SiO$_2$-prS-PdNPs resulting in a decrease in the catalytic activity. A similar phenomenon was observed for HRP and some other nanozymes with peroxidase-like activity at high concentrations of H$_2$O$_2$ and TMB.[27,28] In Fig. 3(e), the effect of increasing the temperature from 25 to 90 °C on the peroxidase-like activity of ITO-SiO$_2$-prS-PdNPs was investigated. The relative activity measured at 652 nm was stable and above 90% up to 70 °C as shown in Fig. 3(e). At high temperatures above 70 °C, the activity drastically decreased and due to the decomposition of H$_2$O$_2$ at high temperatures. The stability of the peroxidase activity of ITO-SiO$_2$-prS-PdNPs was high compared to natural enzymes which has a narrow window of activity.

3.6 Confirming the enzyme-like mechanism of ITO-SiO$_2$-prS-PdNPs

The mechanism of the peroxidase-like activity of nanozymes can proceed *via* either the generation of reactive oxygen radical species such as O$_2^{-\bullet}$, HO$_2^{-\bullet}$, and HO$^{-\bullet}$ or the electron-transfer mechanism.[26] First, we investigated the generation of ROS using the oxygen radical (O$_2^{-\bullet}$) and the singlet oxygen (^{1}O$_2$) quencher DPBF. The absorption of DPBF at 420 nm shown in Fig. S5(a) (ESI†) is expected to decrease due to the generated ROS. There was no change in the intensity of DPBF for up to 10 min in Fig. S5(b) (ESI†), confirming that no ROS was generated. A similar study was investigated using terephthalic acid as a hydroxyl radical trap. No fluorescence signal was observed and therefore no hydroxyl radical was generated. In order to verify whether ITO-SiO$_2$-prS-PdNP peroxidase-like activity originates from the electron-transfer mechanism its electrocatalytic behavior towards H$_2$O$_2$ was investigated using chronoamperometric measurements. Fig. S5(c) (ESI†) shows the chronoamperomogram of ITO-SiO$_2$-prS-PdNPs upon the successive addition of 100 μL of 0.10 mM H$_2$O$_2$ (indicated by arrows) with stirring and a working potential of +0.50 V (*vs.* Ag|AgCI) in acetate buffer (0.10 M, pH 4.0). The current response increases steadily due to electrocatalytic oxidation. The oxidation of H$_2$O$_2$ results in the reduction of PdNPs which then oxidize TMB to blue-coloured products as shown in Scheme 2. Therefore, the peroxidase-like activity of ITO-SiO$_2$-prS-PdNPs was
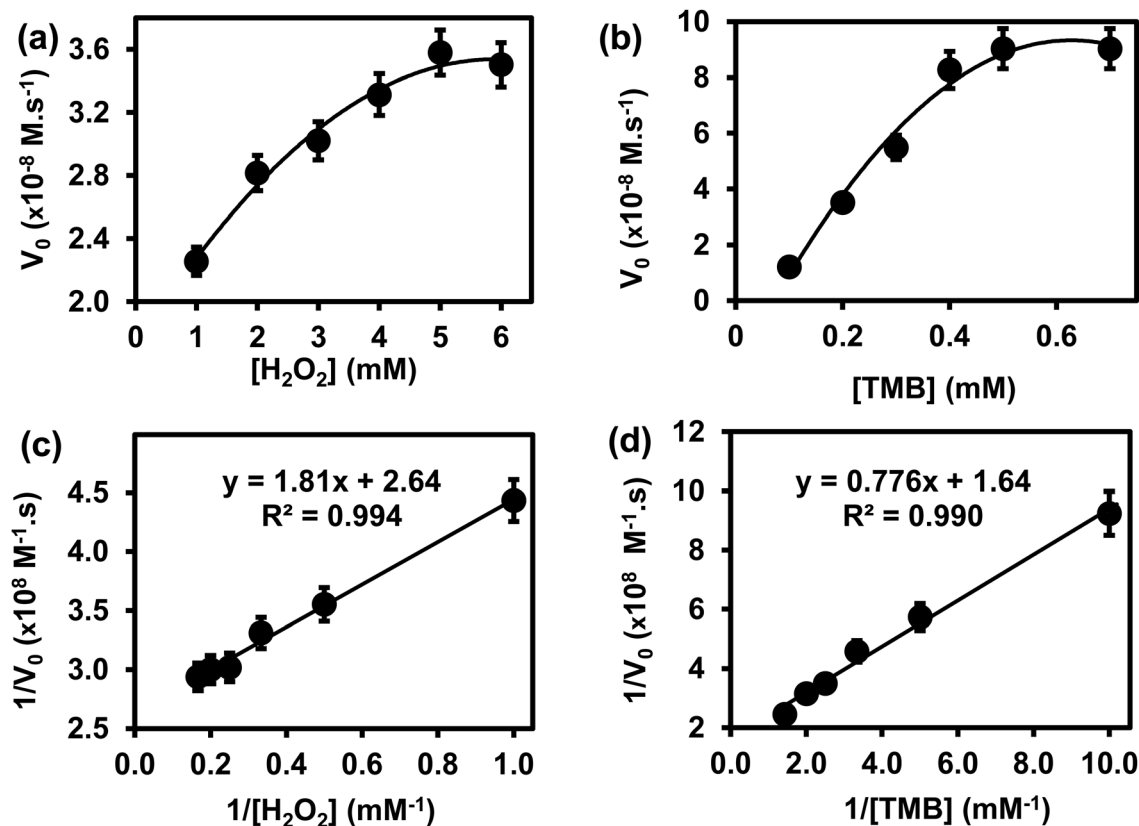

Fig. 4 The steady-state kinetic plots of the ITO-SiO$_2$-prS-PdNPs (a) varying [H$_2$O$_2$] at a fixed [TMB], (b) varying [TMB] at a fixed [H$_2$O$_2$] and their corresponding double reciprocal plots (c) [H$_2$O$_2$] at a fixed [TMB] and (d) [TMB] at a fixed [H$_2$O$_2$].

This journal is © The Royal Society of Chemistry 2023

J. Mater. Chem. B, 2023, **11**, 7961–7971 | **7967**

Table 1 Comparison of the kinetic parameters (K_m and V_{max}) for the peroxidase-like activity of ITO-SiO$_2$-prS-PdNPs with HRP and other previously reported nanozymes

Nanozymes	K_m (mM)		V_{max} ($\times 10^{-8}$ M s^{-1})	
	H$_2$O$_2$	TMB	H$_2$O$_2$	TMB
ITO-SiO$_2$-prS-PdNPs[TW]	0.68	0.47	3.79	6.10
CuO–Au nanoallaoys[9]	4.08	3.54	0.0105	0.0111
HRP[25]	3.7	0.43	8.71	10.0
CuONRs@Pd$_6$NPs[29]	2.94	3.74	1.23	1.65
MnSe-g-C$_3$N$_4$[30]	0.62	0.137	2.85	2.40
Cu/ZnO[31]	71.0	10.0	0.30	2.87

TW-this work.

attributed to the electron-transfer mechanism and similar to the natural horse-radish peroxidase enzyme.

3.7 Steady-state kinetic analysis of ITO-SiO$_2$-prS-PdNPs

The steady-state kinetics was investigated on H$_2$O$_2$ and TMB substrates. The peroxidase-like activity of ITO-SiO$_2$-prS-PdNPs was further investigated by varying the concentration of H$_2$O$_2$ at constant TMB and *vice versa*. A series of initial rates (V_0) for TMB oxidation were obtained from the time-dependent absorption value at 652 nm. The absorbance values were converted to the concentration using the molar absorption coefficient (ε) of oxidized TMB (oxTMB) at 652 nm using eqn (1):

$$[\text{oxTMB}] = \frac{A}{\varepsilon L} \qquad (1)$$

where A is the absorbance at 652 nm, ε is the molar absorption of oxidized TMB at 652 nm (39 000 M^{-1} cm^{-1}), and L is the path length (1 cm).[26,27] In Fig. 4(a), the plot of initial rates (V_0) against the concentrations of substrate H$_2$O$_2$ and TMB (in Fig. 4(b)) was evaluated. The graphs showed an increase in V_0 with the increasing concentration of [H$_2$O$_2$] in Fig. 4(a) and [TMB] in Fig. 4(b). The graphs reached a plateau at high concentrations, 5.0 mM for H$_2$O$_2$ and 0.50 mM for TMB. This confirmed the typical Michaelis–Menten enzyme-like behaviour for the ITO-SiO$_2$-prS-PdNPs. The double reciprocal plots in Fig. 4(c) for H$_2$O$_2$ and (d) for TMB were plotted and used to calculate the K_m value from the slope and V_{max} from the
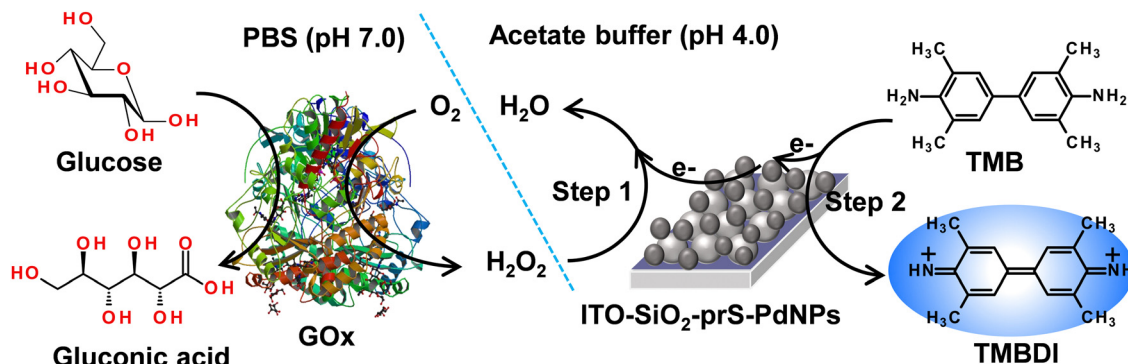
y-intercept using eqn (2):

$$\frac{1}{V_0} = \frac{K_m}{V_{max}} \frac{1}{[S]} + \frac{1}{V_{max}} \qquad (2)$$

where V_0 is the initial rate, V_{max} is the maximal reaction rate, $[S]$ is the concentration of the substrate (H$_2$O$_2$ or TMB), and K_m is the Michaelis–Menten constant. The affinity between the enzyme and the substrate is defined by K_m. The high K_m value indicates a weak affinity, whereas the low K_m value suggests a strong affinity. The calculated kinetic parameters of ITO-SiO$_2$-prS-PdNPs and the comparison with HRP and other nanozymes are summarized in Table 1. The K_m value of ITO-SiO$_2$-prS-PdNPs with H$_2$O$_2$ as the substrate was 0.68 mM and was lower than that of HRP (3.70 mM).[25] Most nanozymes, such as CuONRs@Pd$_6$NPs (2.94 mM)[29] and CuO–Au nanoalloys (4.08 mM),[9] had K_m values higher than ITO-SiO$_2$-prS-PdNPs. Comparable K_m values were observed for MnSe-g-C$_3$N$_4$ (0.62 mM),[30] indicating that ITO-SiO$_2$-prS-PdNPs has a greater affinity for H$_2$O$_2$. On the other hand, the K_m value of the ITO-SiO$_2$-prS-PdNPs using TMB as the substrate was 0.47 mM and was comparable to that of HRP (0.43 mM),[25] but significantly lower than those of other nanozymes such as CuO–Au nanoalloys (3.54 mM),[9] and Zn–CuO (10 mM),[31] suggesting that ITO-SiO$_2$-prS-PdNPs have a high affinity for TMB. The excellent affinity of ITO-SiO$_2$-prS-PdNPs compared to HRP and other reported nanozymes is due to the use of PdNPs and their homogeneous distribution on the SiO$_2$NP surface.

3.8 Colorimetric detection of glucose using ITO-SiO$_2$-prS-PdNPs

The peroxidase-like activity exhibited by ITO-SiO$_2$-prS-PdNPs as nanozymes was used for the potential application of glucose detection. (a) Glucose was oxidized by GOx to form gluconic acid and H$_2$O$_2$ is produced as an enzyme reaction by-product. (b) The produced enzymatic H$_2$O$_2$, in the presence of ITO-SiO$_2$-prS-PdNPs oxidize TMB to its blue-coloured products, oxTMB, as illustrated in Scheme 3.

The intensity of the blue-coloured products at 652 nm was proportional to the concentration of glucose. Fig. 5(a) shows an increase in the UV-vis absorption spectra at 652 nm as the concentration of glucose increased and the calibration curve is shown in Fig. 5(b). The response was linear up to 30 μM. At a

Scheme 3 Schematic representation of the colorimetric determination of glucose using ITO-SiO$_2$-prS-PdNPs.

7968 | *J. Mater. Chem. B*, 2023, **11**, 7961–7971

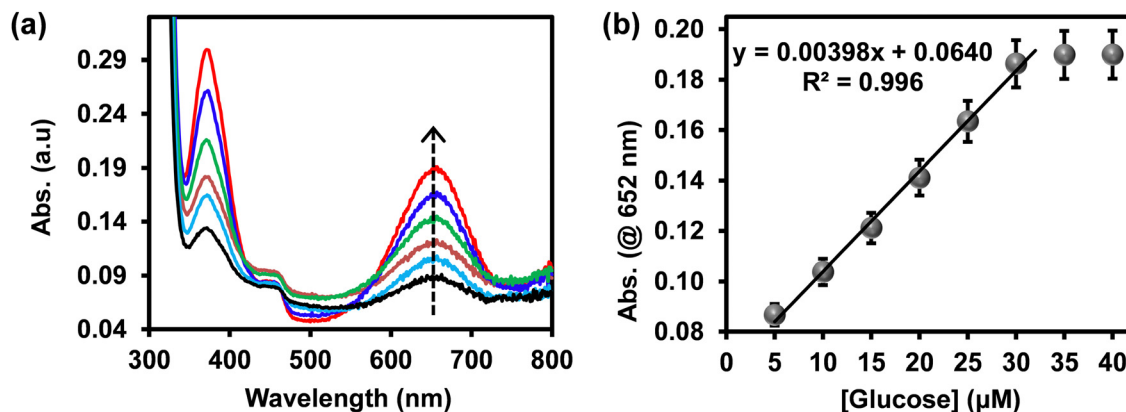This journal is © The Royal Society of Chemistry 2023

Fig. 5 (a) UV-vis absorption spectra and (b) the corresponding linear calibration curve of glucose detection using ITO-SiO$_2$-prS-PdNPs.

higher concentration of glucose, the catalytic activity of ITO-SiO$_2$-prS-PdNPs formed a plateau due to the saturation of catalytic sites on our ITO-SiO$_2$-prS-PdNPs, thus similar absorption intensity. The limit of detection (LoD) and limit of quantification (LoQ) were calculated to be 1.84 μM and 6.14 μM, respectively, using the 3S$_b$/slope for LoD, and the 10S$_b$/slope for LoQ, S$_b$ is the standard deviation of the blank samples (n = 10) and the slope was from Fig. 5.[32] Compared with other nanozymes for glucose sensing our proposed colorimetric method using ITO-SiO$_2$-prS-PdNPs showed better or comparable limit of detection and linear range as summarized in Table 2.

3.9 Selectivity studies

The selectivity analysis of ITO-SiO$_2$-prS-PdNPs for glucose detection was investigated using glucose analogues in place of glucose (0.50 mM). The glucose analogues (fructose, lactose and sucrose) were dissolved in phosphate buffer and kept at a concentration of 5.0 mM. As shown in Fig. 6(a), a blue colour was observed only in the presence of glucose, but not observed for fructose, lactose and sucrose even though the concentrations of these glucose analogues were 10-fold more than glucose. The results showed that our proposed ITO-SiO$_2$-prS-PdNPs as glucose sensors have high selectivity towards glucose. The high selectivity was attributed to the high affinity and specificity of GOx for glucose.

3.10 Reusability of ITO-SiO$_2$-prS-PdNPs for glucose detection

The reusability of ITO-SiO$_2$-prS-PdNPs for glucose detection was investigated by repeating the detection of 15.0 μM glucose for
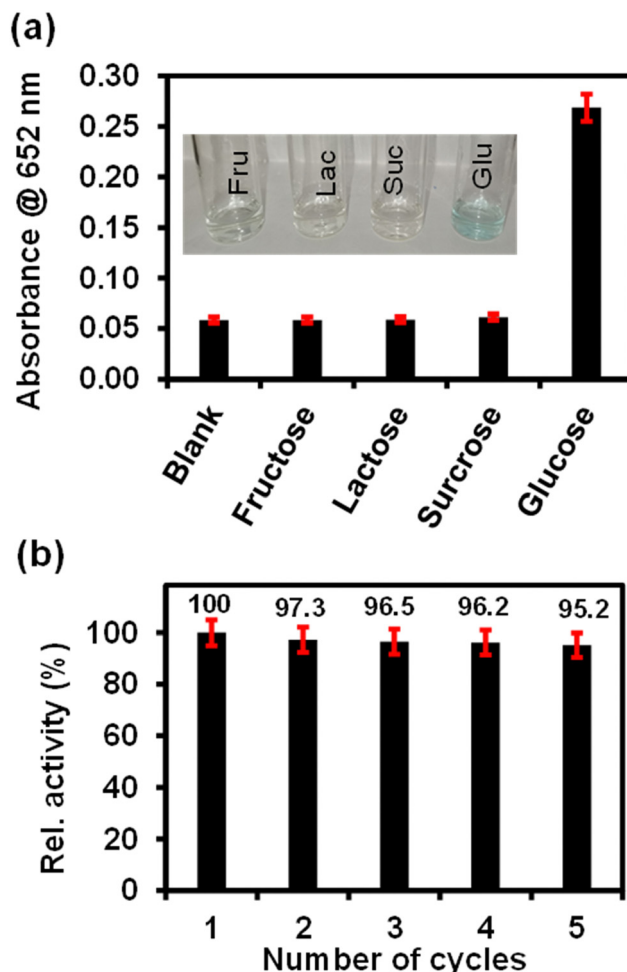

Fig. 6 (a) Selectivity of the colorimetric assay for glucose detection and other interfering substances for ITO-SiO$_2$-prS-PdNPs (inset: The corresponding images of the reaction solutions) and (b) reusability of ITO-SiO$_2$-prS-PdNPs towards the detection of glucose.

5 successful cycles. After each measurement, the ITO-SiO$_2$-prS-PdNPs were removed from the detection solution and washed several times with ethanol, methanol, and Milli-Q water. The recovered ITO-SiO$_2$-prS-PdNPs were reused for glucose

Table 2 Comparison of ITO-SiO$_2$-prS-PdNPs for the colorimetric detection of glucose with other nanozyme-based glucose biosensors

Nanozymes	Linear range (μM)	LoD (μM)	LoQ (μM)
ITO-SiO$_2$-pr-PdNPs[TW]	5–30	1.84	6.14
CuO–Au nanoalloys[9]	0–30	6.80	—
CuONRs@Pd$_6$NPs[29]	0–70	8.87	39.9
GO–COOH[33]	1–20	1.00	—
Cu-Ag/rGO[34]	1–30	3.80	—

TW-this work.

Table 3 Detection of glucose in the 10% NCS ($n = 3$) using the % recovery method and linear curve in Fig. 5(b)

Sample	Added [Glucose] μM	Detected [Glucose] μM	Recovery (%)	RSD (%)
10% NCS + 4.0 μM glucose	4.0	3.7	92.5	3.04
10% NCS + 10.0 μM glucose	10.0	9.7	97.0	2.12
10% NCS + 15.0 μM glucose	15.0	15.8	105.3	3.17

detection in the next cycle. Fig. 6(b) shows that about 95.2% of the peroxidase-like activity of glucose detection by ITO-SiO$_2$-prS-PdNPs after 5 successive cycles was retained with a relative standard deviation (RSD) value of 1.90%, which indicates the feasibility of ITO-SiO$_2$-prS-PdNPs for glucose detection for practical applications.

3.11 Colorimetric detection of glucose in the newborn calf serum (NCS)

Our proposed colorimetric sensor (ITO-SiO$_2$-prS-PdNPs) was further evaluated for glucose detection in real samples, that is in 10% newborn calf serum (NCS). The 10% NCS was spiked with known concentrations of glucose. As listed in Table 3, the % recovery of glucose in 10% NCS was between 92.5 and 105.3%. The percentage relative standard deviation (%RSD) values were between 2.12 and 3.17%. The results showed the feasibility and reliability of the proposed ITO-SiO$_2$-prS-PdNPs as the colorimetric sensor for detecting glucose in the 10% NCS.

4 Conclusions

The preparation of SiO$_2$NPs and PdNPs was successful. The fabricated nanomaterials (SiO$_2$NPs and PdNPs) were used to fabricate ITO-SiO$_2$-prS-PdNPs which exhibited intrinsic peroxidase-like activity. The optimum environmental conditions for the peroxidase-like activity of ITO-SiO$_2$-prS-PdNPs were obtained at pH 4 and < 70 °C. A typical Michaelis–Menten enzyme-like behaviour was observed for the ITO-SiO$_2$-prS-PdNPs using steady-state kinetic analysis. The ITO-SiO$_2$-prS-PdNPs showed good affinity for both H$_2$O$_2$ (K_m 0.68 mM) and TMB (K_m 0.47 mM) compared to that for HRP and other previously reported peroxidase-mimetics. The mechanism of the peroxidase-like activity of ITO-SiO$_2$-prS-PdNPs was confirmed *via* an electron-transfer mechanism between H$_2$O$_2$ and TMB. ITO-SiO$_2$-prS-PdNPs were used as glucose sensors and showed good specificity and selectivity towards glucose in a linear range between 5.0 and 30 μM, LoD (1.84 μM) and LoQ (6.14 μM). Our proposed colorimetric glucose sensor based on ITO-SiO$_2$-prS-PdNPs was simple and easy to recover for glucose detection. Real sample analysis using 10% (NCS) samples confirmed the reliability for glucose detection in practical applications.

Author contributions

Ridge Chavalala: conceptualization, methodology, formal analysis, investigation, and writing–original draft preparation.

Philani Mashazi: supervision, conceptualization, investigation, validation, and writing–reviewing and editing.

Conflicts of interest

There are no conflicts to declare.

Acknowledgements

References

1 J. Wang, *Electrochemical Sensors, Biosensors and their Bio-medical Applications*, Elsevier, 2008, vol. 108, pp. 57–69.

2 A. K. Dutta, S. K. Maji, A. Mondal, B. Karmakar, P. Biswas and B. Adhikary, *Sens. Actuators, B*, 2012, **173**, 724–731.

3 Q. Wu, L. Wang, H. Yu, J. Wang and Z. Chen, *Chem. Rev.*, 2011, **111**, 7855–7875.

4 T. Cai, Y. Gao, J. Yan, Y. Wu and J. Di, *RSC Adv.*, 2017, 7, 29122–29128.

5 K. J. Cash and H. A. Clark, *Trends Mol. Med.*, 2010, **16**, 584–593.

6 U. Alam, O. Asghar, S. Azmi and R. A. Malik, *General aspects of diabetes mellitus*, Elsevier B. V., 2014, vol. 126.

7 R. A. Tromans, S. K. Samanta, A. M. Chapman and A. P. Davis, *Chem. Sci.*, 2020, **11**, 3223–3227.

8 S. Ferri, K. Kojima and K. Sode, *J. Diabetes Sci. Technol.*, 2011, **5**, 1068–1076.

9 S. Mvango and P. Mashazi, *Mater. Sci. Eng., C*, 2019, **96**, 814–823.

10 J. M. Harris, C. Reyes and G. P. Lopez, *J. Diabetes Sci. Technol.*, 2013, **7**, 1030–1038.

11 S.-J. Bao, C. M. Li, J.-F. Zang, X.-Q. Cui, Y. Qiao and J. Guo, *Adv. Funct. Mater.*, 2008, **18**, 591–599.

12 W. Yang, J. Li, M. Wang, X. Sun, Y. Liu, J. Yang and D. H. L. Ng, *Colloids Surf., B*, 2020, **188**, 110742.

13 Y. Bai, W. Yang, Y. Sun and C. Sun, *Sens. Actuators, B*, 2008, **134**, 471–476.

14 L. Meng, J. Jin, G. Yang, T. Lu, H. Zhang and C. Cai, *Anal. Chem.*, 2009, **81**, 7271–7280.

15 H. Tang, J. Chen, S. Yao, L. Nie, G. Deng and Y. Kuang, *Anal. Biochem.*, 2004, **331**, 89–97.

16 Q. Zhang, C. M. Cobley, J. Zeng, L.-P. Wen, J. Chen and Y. Xia, *J. Phys. Chem. C*, 2010, **114**, 6396–6400.

17 H. He, X. Xu, H. Wu and Y. Jin, *Adv. Mater.*, 2012, **24**, 1736–1740.

18 C. Gao, H. Zhu, J. Chen and H. Qiu, *Chin. Chem. Lett.*, 2017, **28**, 1006–1012.

7970 | *J. Mater. Chem. B*, 2023, **11**, 7961–7971

This journal is © The Royal Society of Chemistry 2023

19 H. Zhang, J. Chen, Y. Yang, L. Wang, Z. Li and H. Qiu, *Anal. Chem.*, 2019, **91**, 5004–5010.

20 J. C. Munyemana, J. Chen, H. Tang, Y. Han, J. Wang and H. Qiu, *ACS Appl. Nano Mater.*, 2021, **4**, 2820–2827.

21 O. Adeniyi, S. Sicwetsha and P. Mashazi, *ACS Appl. Mater. Interfaces*, 2020, **12**, 1973–1987.

22 R. Chavalala and P. Mashazi, *ACS Appl. Nano Mater.*, 2023, **6**, 190–199.

23 Z. Ran and W. Yang, *RSC Adv.*, 2014, **40**, 37921–37927.

24 Q. Wang, X. Cui, J. Chen, X. Zheng, C. Liu, T. Xue, H. Wang, Z. Jin, L. Qiao and W. Zheng, *RSC Adv.*, 2012, **2**, 6245–6249.

25 L. Gao, J. Zhuang, L. Nie, J. Zhang, Y. Zhang, N. Gu, T. Wang, J. Feng, D. Yang, S. Perrett and X. Yan, *Nat. Nanotechnol.*, 2007, **2**, 577–583.

26 L. Chen, X. Li, J. Zhang, J. Fang, Y. Huang, P. Wang and J. Ma, *Environ. Sci. Technol.*, 2015, **49**, 10373–10379.

27 Y. Yang, D. Shen, Y. Long, Z. Xie and H. Zheng, *Sci. Rep.*, 2017, **7**, 43141.

28 Y. Liu, G. Zhu, J. Yang, A. Yuan and X. Shen, *PLoS One*, 2014, **9**, e109158.

29 S. Sicwetsha, O. Adeniyi and P. Mashazi, *RSC Adv.*, 2021, **11**, 28818–28828.

30 L. Su, J. Feng, X. Zhou, C. Ren, H. Li and X. Chen, *Anal. Chem.*, 2012, **84**, 5753–5758.

31 F. Qiao, Q. Qi, Z. Wang, K. Xu and S. Ai, *Sens. Actuators, B*, 2016, **229**, 379–386.

32 A. P. Nagvenkar and A. Gedanken, *ACS Appl. Mater. Interfaces*, 2016, **8**, 22301–22308.

33 Y. Song, K. Qu, C. Zhao, J. Ren and X. Qu, *Adv. Mater.*, 2010, **22**, 2206–2210.

34 G. Darabdhara, B. Sharma, M. R. Das, R. Boukherroub and S. Szunerits, *Sens. Actuators, B*, 2017, **238**, 842–851.

This journal is © The Royal Society of Chemistry 2023

J. Mater. Chem. B, 2023, **11**, 7961–7971 | **7971**